Journal of Materials Chemistry B

ROYAL SOCIETY OF CHEMISTRY

PAPER

View Article Online
View Journal | View Issue

Cite this: J. Mater. Chem. B, 2022, 10, 915

A low-swelling and toughened adhesive hydrogel with anti-microbial and hemostatic capacities for wound healing†

Liwei Zhang, [ab] Yajie Zhang, [a] Fanshu Ma,[a] Xingzhu Liu, [a] Yangzhong Liu, [c] Yi Cao *[a] and Renjun Pei*[a]

Received 27th August 2021,
Accepted 4th January 2022

DOI: 10.1039/d1tb01871j

rsc.li/materials-b

Hydrogel-based wound dressings with tissue adhesion abilities are widely used for wound closure. However, currently developed hydrogel adhesives are still poor at continuing to seal wounds while bleeding is ongoing. Herein, we demonstrate an antibacterial and hemostatic hydrogel adhesive with low-swelling properties and toughness for wound healing. The hydrogel was composed of Pluronic F127 diacrylate, quaternized chitosan diacrylate, silk fibroin, and tannic acid, and it was not only able to maintain good tissue adhesion abilities in a moist environment but it also showed guaranteed tissue adhesion and mechanical strength after absorbing water due to its low-swelling and toughness properties. Furthermore, *in vitro* and *in vivo* tests demonstrated that the hydrogel also had antibacterial, antioxidant, and hemostatic properties, which could promote tissue regeneration. All these findings demonstrate that this hydrogel with multifunctional properties is a promising material for clinical wound healing applications.

1. Introduction

The skin is the largest organ of the human body and the first barrier to entry. However, wounds, including acute, chronic, and surgical traumas, are unavoidable in daily life. Additionally, open wounds usually require prolonged healing times and can be a great infection risk.[1,2] Thus, it is essential to employ an adhesive dressing to seal wounds, preventing blood outflow and avoiding bacterial invasion. To date, several commercial tissue adhesive dressings have been developed for wound treatment.[3–6] Unfortunately, they still show some obvious defects. Typically, fibrin glues exhibit limited mechanical stability and tissue adhesion abilities.[7,8] Moreover, cyanoacrylate-based adhesive wound dressings are associated with tissue inflammation, cell necrosis, and cytotoxicity.[9,10] Therefore, adhesive wound dressings that are biocompatible and possess both favorable adhesion abilities and mechanical strength should be developed with urgency.

Hydrogel is a soft material with a high water content that possesses a 3D network structure featuring a large number of hydrophilic groups.[4,11] When a hydrogel is applied as a wound dressing, the special porous structure can facilitate the exchange of nutrients and gases, absorb exudate, and maintain a moist environment, conditions that have been proven to accelerate the healing process of wounds.[12–15] In addition, hydrogels also have many physical and chemical properties that are similar to the extracellular matrix (ECM), promoting cell proliferation, adhesion, migration, and differentiation during the wound healing process.[11,13,16,17] All the merits mentioned above make hydrogels some of the best candidates to act as adhesive wound dressings. To date, many hydrogel adhesives have been developed for dressing wounds arising from trauma and surgical interventions.[3,7,8,18,19] However, most hydrogel adhesives tend to detach from the wound site in moist environments due to reduced mechanical and tissue adhesion properties after swelling;[20] this is inconvenient for practical applications. Consequently, the development of a hydrogel adhesive with low swelling and appropriate mechanical strength is desirable for wound treatment.

Tannic acid (TA) is a polyphenol compound that can interact with various polymers, such as Pluronic F127 (PEO_{99}–PPO_{65}–PEO_{99}),[3] chitosan,[21] silk fibroin (SF),[22] gelatin,[23] and so on, to form hydrogen bonds; it can be used in the fabrication of low-swelling hydrogels and can significantly improve the mechanical and adhesive properties of hydrogels.[19,24] Moreover, it has been

[a] CAS Key Laboratory for Nano-Bio Interface, Suzhou Institute of Nano-Tech and Nano-Bionics, Chinese Academy of Sciences, Suzhou, 215123, China. E-mail: ycao2014@sinano.ac.cn, rjpei2011@sinano.ac.cn
[b] Nano Science and Technology Institute, University of Science and Technology of China, Suzhou, 215123, China
[c] Department of Chemistry, University of Science and Technology of China, Hefei, 230026, China

† Electronic supplementary information (ESI) available. See DOI: 10.1039/d1tb01871j

proved that the abundance of benzene rings in TA provides hydrogels with great adhesion under wet conditions.[19] So far, TA-based hydrogels have been developed as adhesives for wounds, in which the hydrophobicity of the surface enables the hydrogel/substrate interface to become water repellent, easing the formation of noncovalent bonds between the wound dressing and tissue.[19,22,24–28] This adhesion was inspired by mussels, and it is very effective, even in the presence of water. For wound adhesives, the excessive outflow of blood from a wound can also adversely influence the adhesive properties. To address this issue, hydrogel adhesives equipped with suitable hemostatic properties that can provide an environment with relatively low levels of bodily fluids for sealing wounds are more desirable. However, few studies involving the development of TA-based hydrogel adhesives have taken the influence of bleeding on adhesion into consideration.[29,30]

Ultimately, when designing hydrogel adhesives for wound healing, the presence of multifunctionality in a single system, including biocompatibility,[31] high tissue adhesion strength,[32] a low swelling index,[33] toughness,[34] hemostasis,[35,36] and antibacterial[8] and antioxidation properties,[37] is more desirable, since wound healing is a multifaceted biological process.[38] In particular, reducing bleeding and inflammatory factors could speed up the process of wound healing. TA is a natural plant-based source of polyphenol compounds with abundant catechol and pyrogallol groups that exhibits biologically compatible antioxidant functionality.[23] Unfortunately, the antibacterial properties of tannic acid are relatively weak.[39] SF is a natural protein extracted from silkworm cocoons and has natural hemostatic abilities.[40] When SF contacts with blood, it can activate coagulation factor XII in the blood, accelerate the endogenous coagulation process, and induce the production of thrombin, thus promoting hemostasis.[35,40] Moreover, quaternized chitosan (QCS) is a derivative of chitosan that not only exhibits excellent water solubility but also induces favorable antibacterial effects.[8,41] Therefore, the simultaneous introduction of SF and QCS when constructing TA-based hydrogel adhesives could be a reasonable strategy for obtaining multifunctionality, including hemostasis, antibacterial properties, and antioxidation abilities, also protecting adhesion in the presence of bleeding.

As shown in Scheme 1, based on TA, we, for the first time, developed a multifunctional hydrogel adhesive with good tissue adhesion, high toughness, low swelling, hemostasis, antibacterial, and antioxidation properties, and it can significantly enhance the efficacy of a hydrogel adhesive for wound healing. Specifically, TA was introduced into a network (Gel) consisting of Pluronic F127, QCS, and SF. Because of the hydrogen bonds between TA and the three above-mentioned components, the mechanical properties of the composite (Gel/TA) were improved. The abundance of catechol and pyrogallol groups in TA provide the Gel/TA hydrogel with good tissue adhesion abilities, and these can still be maintained in a humid environment because of the low swelling index of the Gel/TA hydrogel. The Gel/TA hydrogel could act as a barrier because of its tissue adhesion properties, preventing blood from flowing out, and the introduction of SF could accelerate the coagulation of blood and further improve the hemostatic abilities of the hydrogel. In addition, the combined action of TA and QCS endowed the Gel/TA hydrogel adhesive with good antibacterial properties. The antioxidation abilities of TA could reduce the production of inflammatory factors in the wound and accelerate the wound healing process. Moreover, based on a skin wound animal model, the Gel/TA hydrogel was demonstrated to be biocompatible and capable of accelerating wound healing compared to commercial tissue adhesives, and it can be applied to the treatment of epidermal wounds.

2. Experimental section

2.1. Materials

Pluronic F127 (PEO_{99}–PPO_{65}–PEO_{99}), acrylic chloride, lithium bromide (LiBr), and deuterated reagents were purchased from Sigma-Aldrich. Chitosan (20 kDa) was purchased from Braunwei. Glycidyl trimethyl ammonium chloride (GTMAC) and methanesulfonic acid were purchased from Adamas. Lithium arylphosphinate (LAP) was obtained from Aladdin. 1,1-Diphenyl-2-picrylhydrazyl (DPPH) was purchased from TCI. Tannic acid, triethylamine (TEA), dichloromethane, and agar powder were obtained from Sinopharm. Yeast and peptone were obtained from Oxoid. Other biological reagents were obtained from Gibco.

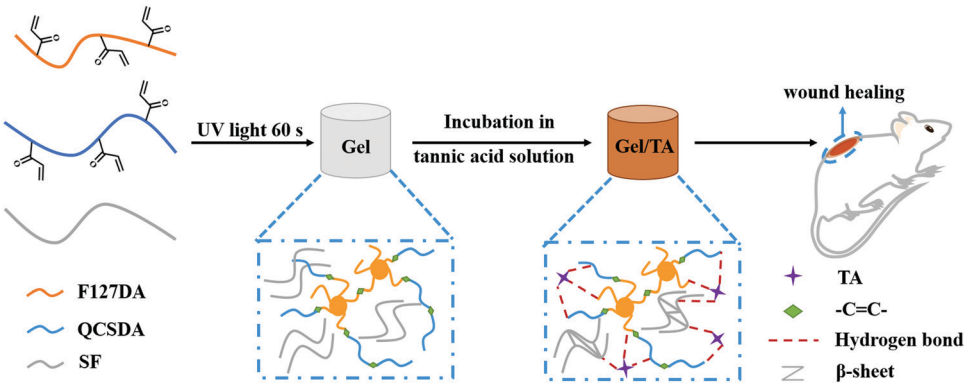

Scheme 1 A schematic diagram of Gel/TA hydrogel adhesive fabrication.

The commercial gel (DuoDERM® Extra Thin Dressing) was obtained from ConvaTec Group PLC.

2.2. Synthesis and characterization of Pluronic F127 diacrylate (F127DA)

F127DA was synthesized *via* an esterification reaction between F127 and acryloyl chloride.[42] Briefly, 5 g of F127 and a ten-fold molar excess of triethylamine were dissolved in 50 mL of dry CH_2Cl_2, followed by adding a ten-fold molar excess of acryloyl chloride in an ice-water bath. After reacting for 24 h, the precipitated triethylammonium chloride was filtered away and the filtrate was precipitated upon addition into excess diethyl ether. The dry crude product was dissolved in 50 mL of deionized water, dialyzed using a dialysis membrane (MWCO: 3.5 kDa) for three days, and lyophilized to obtain pure F127DA. The chemical structure of F127DA was characterized based on ^{1}H-NMR spectroscopy in $CDCl_3$.

2.3. Synthesis and characterization of QCSDA

QCS was synthesized based on a literature method with some modifications.[43] Briefly, 2 g of chitosan was suspended in 72 mL of deionized water, and then 360 μL of acetic acid (0.5% v/v) was added to the suspension. Under continuous stirring at 55 °C, glycidyl trimethylammonium chloride (GTMAC) was dripped into the above mixture over 30 min. Then, the mixture was kept at 55 °C to allow an overnight reaction. Undissolved polymer was removed *via* centrifugation at 4500 rpm for 20 min at room temperature. The supernatant was precipitated in a pre-cooled acetone/ethyl alcohol mixture (1 : 1, v/v) three times. The final product was dried under vacuum. The chemical structure of QCS was characterized *via* ^{1}H-NMR spectroscopy in D_2O.

QCSDA was synthesized according to a literature method with some modifications.[36] Briefly, 400 mg of QCS was dissolved in 60 mL of methanesulfonic acid at room temperature. Then, 1 mL of acryloyl chloride was added dropwise at 0 °C, the reaction was then allowed to proceed under stirring for 1 h at 0 °C and for another 5 h at room temperature. The reaction was then terminated *via* adding crushed ice into the reaction mixture. The solution was purified *via* dialysis against deionized water using dialysis tubing (MWCO: 14 kDa) for 3 days, followed by lyophilization to obtain QCSDA. The chemical structure of QCSDA was characterized based on ^{1}H-NMR spectroscopy in D_2O.

2.4. Synthesis and characterization of SF

Clean silkworm cocoons were added to 0.02 M Na_2CO_3 solution and boiled twice in a water bath at 100 °C for at least 40 min each time to remove sericin. Then, the degummed silk fiber was washed several times with deionized water and dried at room temperature. Then, the silk fibroin was dissolved in 9.3 M LiBr at 60 °C for 4 h. After the solution was cooled to room temperature, the solution was purified *via* dialysis (MWCO: 14 kDa) for 3 days, and it was then lyophilized to obtain SF. The chemical structure of SF was characterized *via* ^{1}H-NMR spectroscopy in D_2O.

2.5. Formation of hydrogels

The two-step method for synthesizing Gel/TA hydrogels was as follows.

(1) Preparation of Gel hydrogels: solutions with 10% F127DA, 2.5% QCSDA, 0.05% LAP, and different concentrations of SF were irradiated under ultraviolet light for 1 min to form hydrogels. Based on the concentration of SF (0%, 0.5%, 1%, and 2%), the hydrogels were named Gel0, Gel0.5, Gel1, and Gel2, accordingly.

(2) Preparation of Gel/TA hydrogels: Gel/TA hydrogels were prepared *via* immersing the Gel hydrogels into a solution of TA (30%) for 4 and 16 h. The hydrogels thus obtained were named Gel0TA4, Gel0.5TA4, Gel1TA4, Gel2TA4, Gel0TA16, Gel0.5TA16, Gel1TA16, and Gel2TA16, accordingly. The Gel/TA hydrogels were repeatedly washed with deionized water prior to use.

2.6. Physiochemical and mechanical properties of hydrogels

Briefly, hydrogels were prepared according to the described procedure. Afterward, they were frozen in liquid nitrogen, followed by lyophilization. The microstructures of the hydrogels were imaged *via* scanning electron microscopy (SEM) with Quanta FEG 250 apparatus at an acceleration voltage of 20.0 kV after gold sputtering.

In order to measure the swelling ratio, hydrogels were swollen in PBS solution (pH = 7.4) at 37 °C until they reached an equilibrium state. The water on the surface of the hydrogel was wiped off, and the weight of the hydrogel was recorded at different times. The swelling ratio was determined using the following equation:

$$\text{Swelling ratio} = (W_S - W_0)/W_0 \times 100\%$$

where W_s is the weight of the swollen sample and W_0 is the weight of the initial sample.

The mechanical properties of the hydrogels were evaluated both *via* rheological and tensile tests. The rheological testing of hydrogels was carried out using a Haake rotational rheometer (RS6000) and the tensile tests were performed using Instron 3365 apparatus.

2.7. Adhesion properties of hydrogels

The adhesion of hydrogels to pork skin was quantitatively measured *via* lap-shear testing. The size of pork skin was 2 cm × 5 cm, and the size of the hydrogel sample was 1.5 cm × 1.5 cm with a thickness of 1 mm. Tissue adhesion was measured using Instron 3365 apparatus with a tensile speed of 10 mm min^{-1}. Moreover, the adhesion properties of hydrogels on different materials (metal (iron), glass, plastic, and wet tissue) were qualitatively evaluated with a digital camera.

2.8. Cytocompatibility testing

WST and live/dead assays were used to evaluate the cytocompatibility of the hydrogels. L929 cells were cultured in RPMI 1640 medium supplemented with 10% fetal bovine serum and 1% penicillin–streptomycin in a CO_2 incubator at 37 °C. Sterilized hydrogel disks were placed into the wells of a

48-well culture plate. Then, L929 fibroblast cells (5×10^3 cells per well) were seeded onto the surfaces of the hydrogels and incubated at 37 °C. The positive control group was the cell culture plate. After 1, 3, and 5 days, WST agent was added into each well and incubation was carried out for 3 h. The optical density (OD) values of the cell suspensions at 450 nm were measured using a microplate reader to evaluate the proliferation of cells. For the live/dead assay, live/dead agent was added. After 20 min, the stained cells were observed *via* fluorescence microscopy (Zeiss Axio Imager Z1, Germany).

2.9. *In vitro* antibacterial activity

Gram-positive Staphylococcus aureus (*S. aureus*) and Gram-negative Escherichia coli (*E. coli*) were employed to test the antibacterial activities of the hydrogels. In brief, hydrogel disks with a diameter of 8 mm and a height of 2 mm were prepared and sterilized with 75% alcohol. Then, the hydrogels were placed in the wells of a 96-well plate and rinsed with sterile PBS. Then, 10 μL of bacterial suspension (in PBS, 10^5 CFU mL^{-1}) was added onto the surfaces of the hydrogel disks. Next, the 96-well plate was incubated in an incubator at 37 °C for 4 h. Finally, 200 μL of sterilized PBS (DPBS) was added to each well to release the surviving bacteria. 10 μL of diluent was added to the agar plate and incubation was carried out at 37 °C overnight. After that, the colony-forming unit (CFU) values were used to evaluate the antibacterial properties of all hydrogels. At the same time, 10 μL of bacterial suspension (10^5 CFU mL^{-1}) added into 200 μL of sterilized DPBS was used as a control group.

2.10. Antioxidant capacity of hydrogels

The antioxidant capacities of the hydrogels were determined *via* measuring the DPPH scavenging capacities.[44] DPPH radical scavenging experiments were performed according to the Blois method.[45] 50 μM DPPH radical solution with ethanol was prepared in advance. Then, the same volume of hydrogel was placed into 200 μL of DPPH radical solution in the dark. After 30 min, the absorbance was measured at 519 nm. An equal volume of deionized water was used instead of the hydrogel as a blank group. The scavenging capacity for DPPH radicals was obtained using the following equation:

$$\text{Scavenging effect } (\%) = \frac{A_{\text{control}} - A_{\text{sample}}}{A_{\text{control}}} \times 100$$

where A_{control} is the absorbance of the blank group and A_{sample} is the absorbance of the experimental group.

2.11. *In vivo* hemostatic performance of hydrogels

A mouse-tail amputation model was used to evaluate the hemostatic capacities of the hydrogels.[46] Animal experiments were reviewed and approved by the Animal Investigation Ethics Committee of the Chinese Academy of Sciences. The mice (ICR, female, 30–40 g) were anesthetized with 10 wt% chloral hydrate (3 mL kg^{-1}), and then a mouse was fixed on a surgical board. Then, the tail of the mouse was cut to half its length with a scalpel. After cutting, the tail of the mouse was left free to ensure the normal release of blood. Then, the wound was covered with the hydrogel (a diameter of 8 mm and a thickness of 2 mm), and the bleeding from the wound was observed. The bleeding time and blood loss were recorded until the wound stopped bleeding. A wound covered with gelatin sponge or commercial gel under slight pressure was used as a positive control. A wound without treatment was used as a negative control.

2.12. *In vivo* wound healing

A rat-based full-thickness cutaneous wound model was employed to evaluate the effects of hydrogels on the wound healing of skin. Animal experiments were reviewed and approved by the Animal Investigation Ethics Committee of the Chinese Academy of Sciences. First, healthy female Sprague–Dawley rats (200–250 g, Nanjing Sikerui Biological Technology Co. Ltd, China) were anesthetized and their backs were shaved. Four rounded full-thickness wound (2 cm in diameter) areas were created on the back of each mouse. Mice were divided into five groups, including a blank control group, a commercial dressing group, a Gel0 group, a Gel2 group, and a Gel2TA16 group (each group contained 4 rats). The blank control group was treated by wrapping with sterile gauze. The wound-healing rates were calculated *via* comparing the healed wound area with the original wound area for the different groups. After 0, 2, 5, 9, 14, and 21 days, photos were taken of wound healing in different groups. After 14 and 21 days of healing, the entire wound area and adjacent normal skin were collected and fixed in 4% paraformaldehyde. After sectioning using paraffin, sections were stained with hematoxylin-eosin (H&E) and Masson's trichrome stain for histological analysis. Different groups of mouse skin tissue sections were observed and analyzed under a microscope.

2.13. Statistical analysis

All experiments were repeated three times. All data in this study are presented as mean ± standard deviation (SD), and experimental data were analyzed using Student's t test, in which a p value < 0.05 was considered statistically significant. *, **, and *** represent $p < 0.05$, $p < 0.01$, and $p < 0.001$, respectively.

3. Results and discussion

3.1. Synthesis and characterization of F127DA, QCSDA, and SF

To prepare the Gel/TA hydrogel, we first synthesized F127DA *via* an esterification reaction between F127 and acryloyl chloride. In the ^{1}H-NMR spectrum of F127DA, new peaks (in the region of 5.8–6.5 ppm) ascribed to double bonds could be observed clearly (Fig. S1, ESI†). In addition, the integration ratio of those peaks in the 5.8–6.5 ppm region to the peak at 1.1 ppm was 0.0189 : 1, which is close to the theoretical value of 0.0205 : 1, indicating that double bonds were successfully introduced at both ends of F127DA.

To synthesize QCSDA, the antibacterial polymer QCS was first synthesized *via* grafting GTMAC to the amino group of chitosan. Then, QCSDA was synthesized *via* a reaction between

QCS and acryloyl chloride. In comparison with the ^{1}H-NMR spectrum of QCS, new peaks (at 3.3 ppm and in the region of 6.0–6.6 ppm) ascribed to GTMAC and double bonds were clearly observed in the spectrum of QCSDA (Fig. S2, ESI†). In addition, SF was extracted from natural silkworm cocoons. As shown in Fig. S3 (ESI†), the ^{1}H-NMR spectrum of SF showed the characteristic peak of lysine (at around 3 ppm) that is indicative of SF, confirming the structure of SF.

3.2. Microstructures and swelling ratios of hydrogels

Gel hydrogels were prepared *via* crosslinking mixtures containing F127DA, QCSDA, and SF under UV light. The hydrogels with different SF concentrations of 0%, 0.5%, 1%, and 2% were named Gel0, Gel0.5, Gel1, and Gel2, respectively. Gel/TA hydrogels were formed *via* soaking the Gel hydrogels in TA solution. Taking Gel0 as an example, the hydrogels with different soaking times of 4 and 16 h were named Gel0TA4 and Gel0TA16, respectively.

As shown in Fig. 1, the gel component of Gel2 was more compact than that of Gel0, which is ascribed to the addition of SF. Additionally, the gel component of the Gel/TA hydrogel was relatively more compact than that of the Gel hydrogel, arising from hydrogen bonds between TA and the Gel hydrogel network. In terms of the hydrogel pores, the average pore size of the Gel2TA16 hydrogel was larger than 50 μm (Fig. S4, ESI†), which was propitious for cell growth.

Moreover, as shown in Fig. 2, it could be found that the TA composite significantly reduced the swelling ratio upon comparing Gel/TA with the Gel hydrogel. Over one day, Gel2 had a swelling ratio of 251%, while Gel2TA16 swelled slightly, with a swelling ratio of 25% (Fig. 2C). The high swelling ratio of Gel2 was due to hydrogen bond interactions between F127DA and H_2O. However, when TA was introduced, the obtained hydrogel exhibited a more compact structure and the penetration of additional water was limited because the hydrogen bond interactions between TA and F127DA were stronger than those between H_2O and F127DA (Fig. 2B). In addition, TA conjugation also endowed the Gel2TA16 hydrogels with a larger water contact angle (59.25 ± 0.79°) compared with the Gel hydrogel (8.85 ± 1.20°) (Fig. S5, ESI†). The increased hydrophobicity could contribute to the reduction in the swelling ratio of the Gel2TA16 hydrogel. During clinical application, a major problem is that swelling due to surrounding fluid results in weakening of the mechanical strength and the adhesion of biological scaffolds or surgical patches.[47,48] Thus, the Gel2TA16 hydrogel with a low swelling ratio is suitable as a wound dressing candidate.

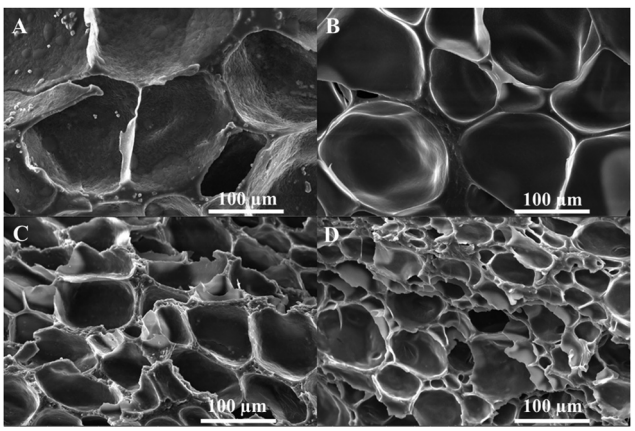

Fig. 1 SEM images of hydrogel morphologies: (A) Gel0, (B) Gel0TA16, (C) Gel2, and (D) Gel2TA16.

3.3. Mechanical properties of hydrogels

To investigate the influence of SF and TA on the viscoelasticity of hydrogels, different kinds of Gel and Gel/TA hydrogels were subject to rheology testing. Oscillatory frequency sweep measurements revealed that the storage modulus (G') values of the Gel hydrogels slightly increased with a rise in frequency, in part because of effects due to the β-sheets of SF upon shearing. With an increase in the SF concentration, the G' values of the Gel hydrogels significantly increased, while the loss modulus (G'') values displayed relatively frequency-independent behavior (Fig. 3A). The enhancement of the G' value was ascribed to an increase in the solid content and the β-sheets of SF. Noticeably, the Gel/TA hydrogels showed special frequency-dependent behavior, where the G' and G'' values increased with a rise in frequency (Fig. 3B). Essentially, the hydrogen bond forces between TA and the other components, including F127DA, QCSDA, and SF, probably resulted in this phenomenon. Moreover, the G' values of hydrogels with higher amounts of SF and TA were similarly higher.

For tensile performance testing, Gel and Gel/TA hydrogel samples were prepared as shown in Fig. 3C. Fig. 3D shows images of the stretching of Gel and Gel/TA hydrogels. The tensile strain of the Gel2 hydrogel was 767%, which was much larger than those of the hydrogels Gel0, Gel0.5, and Gel1 (307%, 323%, and 461%, respectively) (Fig. 3E). In a word, the Gel2 hydrogel showed favorable elastic properties due to the addition of SF. Generally, adding a dissipative layer into a hydrogel network can make it more ductile. Furthermore, as the amount of SF increased, the tensile stress of the hydrogel also increased. In addition, after the introduction of TA, the hydrogen bonding forces between TA molecules and other components in the Gel/TA hydrogel further increased the tensile stress of the hydrogel, however, the elongation was simultaneously reduced (as shown in Fig. 3E and F). Comparing the above hydrogels, Gel2TA16 possessed the largest tensile stress (76.22 kPa) and good elongation (629%). In summary, the Gel2TA16 hydrogel possesses favorable mechanical properties.

3.4. Adhesive properties of hydrogels

Ideal wound dressings should possess excellent tissue adhesion properties so that they can attach to wounds without falling off and provide a protection barrier. To measure the adhesion strengths of Gel/TA hydrogels with different concentrations of SF and different TA soaking times, samples were prepared as shown in Fig. 4A. As shown in Fig. 4B, with an increase in the SF concentration and the TA soaking time, the adhesion strength of hydrogel on porcine skin became stronger. The Gel2TA16

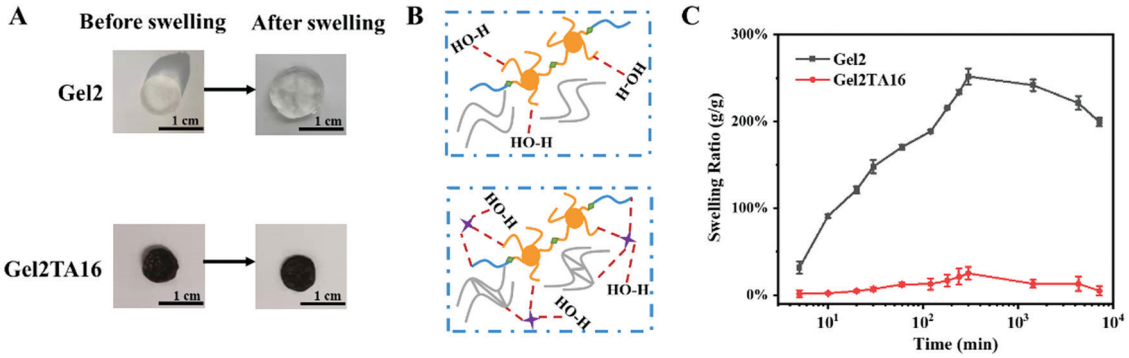

Fig. 2 The swelling behaviors of the hydrogels: (A) photos of the hydrogels Gel2 and Gel2TA16 before and after swelling; (B) schematic diagrams of the swelling principles for hydrogels Gel2 and Gel2TA16; and (C) the swelling ratios of the hydrogels Gel2 and Gel2TA16 (mean ± SD, n = 3).

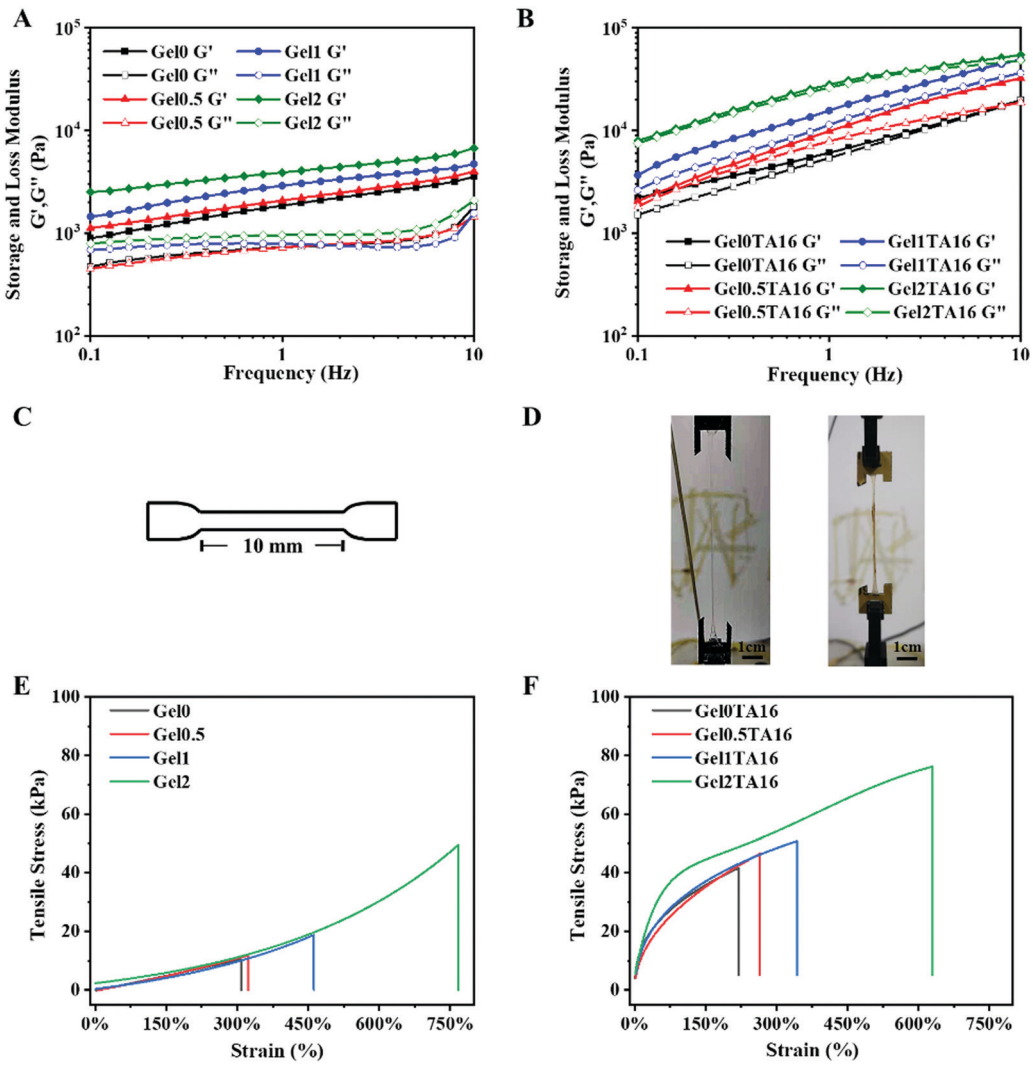

Fig. 3 The mechanical properties of the hydrogels: the rheological properties of (A) gel and (B) gel/TA hydrogels; (C) a diagram of a tensile test strip; (D) images of tensile testing; and the tensile stress data for (E) gel and (F) gel/TA hydrogels.

hydrogel exhibited the best tissue adhesion strength (23.45 ± 3.67 kPa), while the adhesion strengths of the hydrogels Gel0TA4, Gel0TA16, and Gel2TA4 were 6.38 ± 1.97 kPa, 11.41 ± 0.99 kPa, and 14.00 ± 1.75 kPa, respectively. Furthermore, the Gel2TA16 hydrogel was shown to have the ability to adhere to a variety of substrates (such as metal (iron), glass,

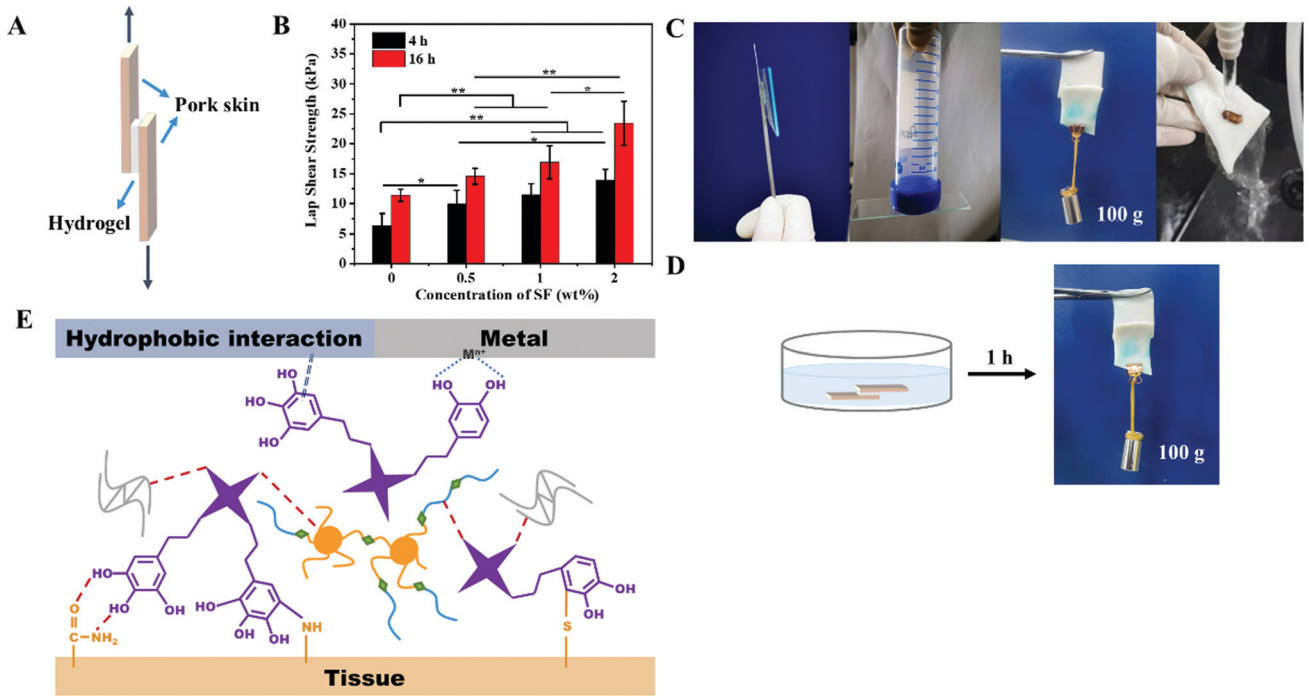

Fig. 4 The adhesive properties of the hydrogels: (A) a schematic diagram of tissue adhesion performance testing; (B) the tissue adhesion strengths of the Gel/TA hydrogels; (C) images of the Gel2TA16 hydrogel adhered to different interfaces (metal (iron), glass, plastic, and wet tissue); (D) a photograph showing the stability during underwater tissue adhesion, where a sample was immersed in water for 1 h; and (E) a schematic diagram of the adhesion mechanism. *$p \leq 0.05$, **$p \leq 0.01$, and ***$p \leq 0.001$; mean ± SD, $n = 5$.

plastic, and wet tissue), as shown in Fig. 4C. Moreover, the adhesion performance of the Gel2TA16 hydrogel in a moist environment showed good stability, as evidenced by the stable adhesion to porcine skin upon being soaked in water for 1 h or being subjected to running water for ten minutes (Fig. 4C and D; Video S1, ESI†). The adhesion mechanism of the Gel/TA hydrogels is illuminated in Fig. 4E. Multiple interactions (interfacial adhesion) between the *o*-phenol groups of TA and the surface (for example, hydrogen bonds, hydrophobic interactions, coordination bonds, and covalent bonds)[22,23] gave the Gel/TA hydrogels adhesive properties, which the Gel hydrogels did not have. This adhesion mechanism was inspired by mussels, whose high adhesion abilities are mainly provided by catechols in the adhesion proteins. Compared with some mussel-inspired adhesive hydrogels, this Gel/TA hydrogel had enough catechol groups on the surface of the hydrogel to ensure good adhesion properties.

For the hydrogels presented in this study, with an increase in the concentration of SF and the soaking time, more hydrogen bonds were formed between TA and the hydrogel components and there were more *o*-phenol groups on the surface of the hydrogel, which resulted in superior adhesion performance. In addition, when the amount of TA in the Gel/TA hydrogel increased, the mechanical strength (cohesion) of the hydrogel was also improved compared with the high-swelling Gel hydrogels (as shown in Fig. 3E and F). Since the Gel hydrogels did not have tissue adhesion properties, another high-swelling hydrogel, AHA/CCS, was used to further prove that the mechanical strength and tissue adhesion of a high swelling-hydrogel are relatively poor (Fig. S6, ESI†). Meanwhile, some high-swelling hydrogels have been previously reported[49,50] whose tissue adhesion strengths were less than 10 kPa. The low-swelling hydrogel we prepared had similar properties to a low-swelling adhesive previously reported.[25] Their tissue adhesion strengths were both more than 20 kPa, and both could maintain tissue adhesion in a moist environment. For adhesive hydrogels used as wound dressings, interface adhesion forces can make them firmly adhere to the tissue surface, while cohesion forces can ensure their stability *via* withstanding mechanical forces from the surrounding tissue. Therefore, the Gel2TA16 hydrogel is suitable for application as a wound dressing.

3.5. Biocompatibility of hydrogels

In order to assess the biocompatibility of the hydrogel, L929 cells were directly seeded onto the surface of the Gel2TA16 hydrogel to examine its cytocompatibility. As shown in Fig. 5A, L929 cells could maintain continuous proliferation during the culturing period from 1 to 5 days. Fluorescence microscopy showed that the surface of the hydrogel could support cell growth and adhesion, and nearly no dead cells (red) were found during culturing (Fig. 5B). Moreover, Fig. 5C shows that L929 cells tended to migrate into the hydrogel during culturing. The above results indicate that Gel2TA16 had no obvious toxic effects towards L929 cells.

3.6. Antibacterial activities of hydrogels

Bacterial infection usually results in slow wound healing and poor healing quality. In addition to having barrier functionality

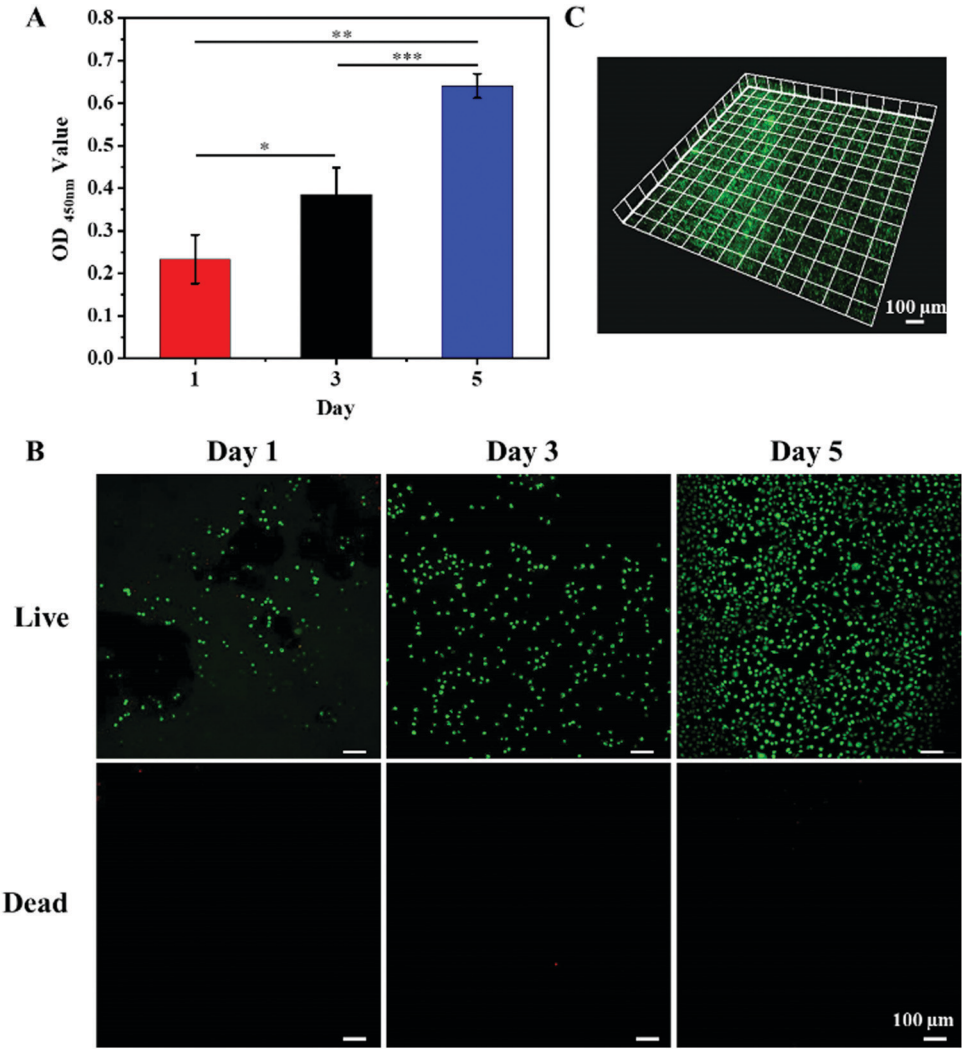

Fig. 5 The biocompatibility of the Gel2TA16 hydrogel: (A) the OD_{450nm} values and (B) live/dead images of L929 cells adhered onto the surface of Gel2TA16 from 1 to 5 days; and (C) a 3D live/dead image of L929 cells adhered onto the surface of Gel2TA16 on day 5. *$p \leq 0.05$, **$p \leq 0.01$, and ***$p \leq 0.001$; mean ± SD, $n = 3$.

to protect wounds from external contamination, wound dressings with inherent antibacterial activity are more attractive. Thus, hydrogel-based wound dressings that possess good antibacterial activity are favorable. As shown in Fig. 6A, *S. aureus* and *E. coli*, representing Gram-positive and Gram-negative bacteria, respectively, were employed to evaluate the antibacterial activities of the hydrogels. Only a few bacterial colonies were observed in the Gel0 and Gel2 hydrogel groups, due to the antibacterial effects arising from the large amount of positive charge from QCSDA. The positively charged quaternary amino groups of QCSDA can electrostatically adsorb and destroy negatively charged bacterial cell membranes, resulting in the release of intracellular fluid, leading to bactericidal effects. Furthermore, when TA was added into the hydrogel, it was found that almost no bacterial colonies were seen in the Gel2TA16 and Gel0TA16 hydrogel groups; this was ascribed to the fact that TA is a natural polyphenol that can inhibit the growth of a variety of bacteria. Additionally, although the F127DA hydrogel group showed fewer bacterial colonies compared with the control group, there were more bacterial colonies compared with the Gel0 and Gel2 hydrogel groups. In the case of the F127DA hydrogel, the porous structure of the hydrogel could filter out some bacteria, but it still did not effectively exhibit antibacterial effects due to a lack of antibacterial ingredients. Overall, since Gel2TA16 was almost 100% resistant to *E. coli* and *S. aureus*, we concluded that it has great potential to be used as an antibacterial biomaterial.

3.7. Antioxidant capacities of hydrogels

For wound healing, the excessive production of reactive oxygen species (ROS) around the wound site can disrupt the balance of oxidants and antioxidants, thus resulting in high levels of inflammatory factors, slow wound healing, and poor healing quality.[34,51,52] As a result, hydrogels for wound healing that show good antioxidant activity are essential. For these hydrogel samples, DPPH scavenging testing was used to determine the antioxidant activity.[52] The active hydrogen atoms of chitosan

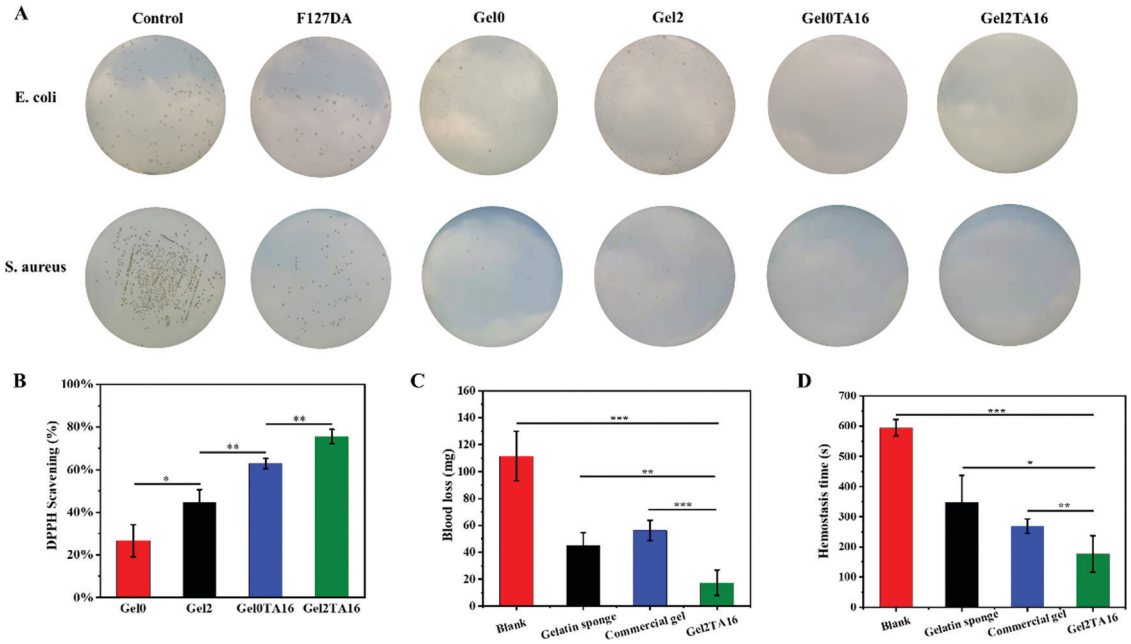

Fig. 6 (A) The antibacterial activities of the hydrogels. (B) The antioxidant capacities of the hydrogels. (C) Blood loss levels and (D) hemostasis times for blank, gelatin sponge, commercial gel, and Gel2TA16 hydrogel groups based on a mouse-tail amputation model. *$p \leq 0.05$, **$p \leq 0.01$, and ***$p \leq 0.001$; mean ± SD, $n = 4$.

can react with hydroxyl and superoxide anion free radicals to form stable macromolecular free radicals, leading to certain free radical scavenging abilities.[53,54] In addition, since serine and tryptophan in silk fibroin contain phenolic side chains, SF also has the ability to scavenge free radicals. As expected, Gel2 (44.70% ± 5.99%) has slightly stronger antioxidant abilities than Gel0 (26.67% ± 7.57%) (as shown in Fig. 6B). Moreover, the large number of phenolic hydroxyl groups in TA could provide hydrogen atoms to reduce DPPH. Thus, the clearance rate in DPPH testing was significantly improved with an increase in the amount of TA in the hydrogel (as shown in Fig. 6B). Gel2TA16 exhibited strong antioxidant activity, with a DPPH free radical scavenging rate of 75.48% ± 3.40%, while the DPPH free radical scavenging rate of Gel0TA16 was 62.92% ± 2.38%. Consequently, DPPH scavenging testing shows that the Gel2TA16 hydrogel has attractive antioxidant activity.

3.8. Study of hemostatic performance

A mouse tail amputation model was used to evaluate hemostasis *in vivo*. The blood loss from blank group mice was 111.7 ± 18.3 mg. After treatment with gelatin sponge, commercial gel, and the Gel2TA16 hydrogel, the blood loss was reduced to 45.2 ± 9.6 mg, 56.3 ± 7.6 mg, and 17.4 ± 9.4 mg, respectively (as shown in Fig. 6C). As shown in Fig. 6D, the hemostasis times of gelatin sponge (347.3 ± 90.6 s), commercial gel (268.3 ± 23.8 s) and the Gel2TA16 hydrogel (176.3 ± 60.3 s) were significantly shorter than that of the blank group (595.7 ± 27.6 s). Gelatin sponge could absorb water in the blood and promote an increase in the concentration of coagulation factors at the wound, while commercial gel is a tissue adhesive that could adhere to the bleeding site to prevent blood from flowing out. The Gel2TA16 hydrogel had the fastest hemostasis time and lowest blood loss, which could be ascribed to its good tissue adhesion performance and the hemostatic abilities of SF and TA. On one hand, Gel2TA16 could firmly adhere to the bleeding site to form a physical barrier and prevent blood from flowing out. On the other hand, when silk fibroin came into contact with blood, Gel2TA16 could activate coagulation factor XII in the blood, accelerate the initiation of the endogenous coagulation pathway, induce the production of thrombin, and promote hemostasis.[40] Furthermore, the phenolic hydroxyl groups of TA could interact with blood and stimulate blood clotting to stop bleeding. Based on these hemostatic mechanisms, Gel2TA16 ultimately exhibited excellent hemostatic abilities compared with gelatin sponge and commercial gel.

3.9. Wound healing

In vivo studies were further carried out to explore the potential wound repair properties of the Gel2TA16 hydrogel, particularly how hydrogels affect healing in a full-thickness wound defect model. The blank group was set as the negative control group, while the commercial gel dressing group, Gel0 hydrogel group, and Gel2 hydrogel group were used as positive control groups. From Fig. 7A and B, it could be clearly found that the wound closure of groups treated with the dressings were better than the blank group, with a lack of scabs appearing during the healing process. Since the application of a dressing can maintain a relatively moist healing environment, absorb wound exudate, and prevent bacterial invasion, it can thereby speed up wound healing. In the first two days, the Gel2TA16 hydrogel performed better in terms of wound closure compared with the other positive control groups. This phenomenon was due to the

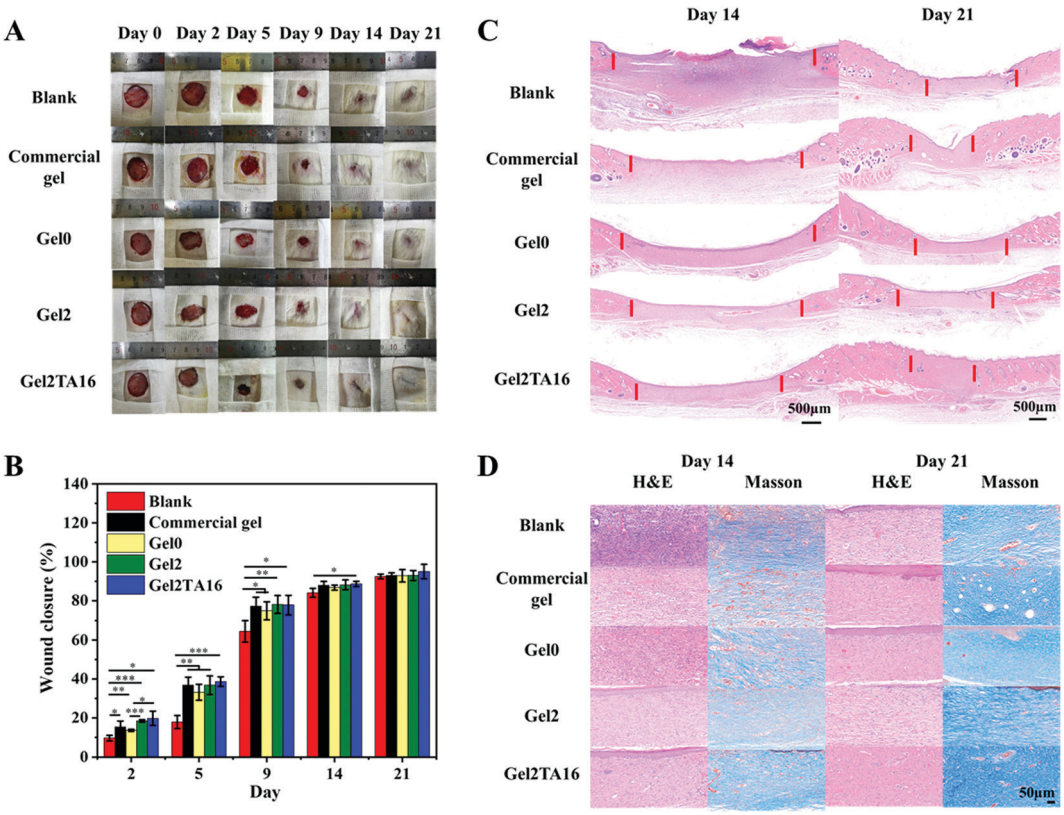

Fig. 7 An evaluation of hydrogel application *in vivo* for wound closure and skin repair: (A) images of wound closure after different periods of healing; (B) wound closure percentages after different periods of healing; (C) H&E staining of wound sections after 14 and 21 days of treatment; and (D) magnified H&E and Masson staining images at the wound bed. $*p \leq 0.05$, $**p \leq 0.01$, and $***p \leq 0.001$; mean ± SD, $n = 4$.

fact that the Gel2TA16 hydrogel had better biological activity (antibacterial, hemostasis, and anti-oxidation) and tissue adhesion properties compared to the other positive control groups, and it allowed the first two stages of the wound healing process (hemostasis and inflammation) to be completed faster. Since commercial gel can provide a moist healing environment for a longer period of time than the hydrogel groups, its closure rate tended to be consistent with the Gel2TA16 hydrogel over the next few days. In the later stages of wound healing, the healing degree of each group tended to be at the same level, and the wounds were basically healed on the 21st day. Noticeably, among these groups, the Gel2TA16 hydrogel group exhibited the smallest unhealed area.

The quality of wound healing was further studied *via* observing the histopathological changes in skin specimens after 14 and 21 days of treatment. The results of hematoxylin-eosin (H&E) staining showed that the unclosed area of the wound treated with the Gel2TA16 hydrogel was the smallest compared with the other groups, and this group showed the most complete skin tissue structure (Fig. 7C). Moreover, the wound treated with the Gel2TA16 hydrogel formed pores, blood vessels, subcutaneous fat, and muscle tissue, while the wounds in the Gel0 and Gel2 hydrogel group showed only low levels of fat and muscle production. The commercial-gel-treated wound began to form fat and muscle layers but the arrangement was not very tight, and the healing quality was not as good as the Gel2TA16 hydrogel group. Additionally, a Masson staining study showed that collagen accumulation at the wound treated with the Gel2TA16 hydrogel was significantly increased and the arrangement was more compact and regular compared with the other groups (as shown in Fig. 7D). Therefore, the Gel2TA16 hydrogel is a potential wound dressing for speeding up wound healing and improving the quality of wound healing.

4. Conclusions

We herein developed a multifunctional hydrogel adhesive with good tissue adhesion properties, high toughness, low swelling, and hemostasis, antibacterial, and antioxidation properties, and it could significantly enhance the efficacy of hydrogel adhesives for wound repair. We explored the effects of the use of various amounts of silk fibroin and different tannic acid soaking times on the mechanical properties and tissue adhesion properties of hydrogels. The results showed that with an increase in the silk fibroin amount and the tannic acid soaking time, the mechanical strength and tissue adhesion abilities of the hydrogels also increased significantly. The introduction of tannic acid made the surface of the hydrogel hydrophobic and simultaneously endowed the hydrogel with a low swelling index, allowing the Gel2TA16 hydrogel to maintain favorable mechanical strength and tissue adhesion abilities in a moist environment. Moreover, for the Gel2TA16 hydrogel, SF

activated the procoagulant cascade and the phenolic hydroxyl groups of TA interacted with blood and stimulated blood coagulation; therefore, the hydrogel showed excellent hemostatic functionality, quickly stopping bleeding after wound closure and promoting wound healing. Additionally, the Gel2TA16 hydrogel had antioxidant and antibacterial capabilities, and it could reduce the production of inflammatory factors during the wound healing process and improve the quality of healing. All the above characteristics make this material an all-in-one hydrogel with multiple functionality that can accelerate wound healing.

Conflicts of interest

There are no conflicts to declare.

Acknowledgements

This work was supported by the Strategic Priority Research Program of the Chinese Academy of Sciences (XDA16040700) and the National Natural Science Foundation of China (No. 31971326).

Notes and references

1 Z. Li, A. Milionis, Y. Zheng, M. Yee, L. Codispoti, F. Tan, D. Poulikakos and C. H. Yap, *Nat. Commun.*, 2019, **10**, 5562.
2 J. Zhu, F. Li, X. Wang, J. Yu and D. Wu, *ACS Appl. Mater. Interfaces*, 2018, **10**, 13304.
3 X. Du, Y. Hou, L. Wu, S. Li, A. Yu, D. Kong, L. Wang and G. Niu, *J. Mater. Chem. B*, 2020, **8**, 5682–5693.
4 L. Zhang, M. Liu, Y. Zhang and R. Pei, *Biomacromolecules*, 2020, **21**, 3966–3983.
5 S. Dhivya, V. V. Padma and E. Santhini, *Biomedicine*, 2015, **5**, 24–28.
6 J. Koehler, F. P. Brandl and A. M. Goepferich, *Eur. Polym. J.*, 2018, **100**, 1–11.
7 Y. Bu, L. Zhang, G. Sun, F. Sun, J. Liu, F. Yang, P. Tang and D. Wu, *Adv. Mater.*, 2019, **31**, 1901580.
8 J. Qu, X. Zhao, Y. Liang, T. Zhang, P. X. Ma and B. Guo, *Biomaterials*, 2018, **183**, 185–199.
9 N. Annabi, D. Rana, E. Shirzaei Sani, R. Portillo-Lara, J. L. Gifford, M. M. Fares, S. M. Mithieux and A. S. Weiss, *Biomaterials*, 2017, **139**, 229–243.
10 R. H. Dong, C. C. Qin, X. Qiu, X. Yan, M. Yu, L. Cui, Y. Zhou, H. D. Zhang, X. Y. Jiang and Y. Z. Long, *Nanoscale*, 2015, **7**, 19468–19475.
11 G. M. Guebitz and G. S. Nyanhongo, *Trends Biotechnol.*, 2018, **36**, 1040–1053.
12 Q. Huang, Y. Zou, M. C. Arno, S. Chen, T. Wang, J. Gao, A. P. Dove and J. Du, *Chem. Soc. Rev.*, 2017, **46**, 6255–6275.
13 J. Li, F. Yu, G. Chen, J. Liu, X.-L. Li, B. Cheng, X.-M. Mo, C. Chen and J.-F. Pan, *ACS Appl. Mater. Interfaces*, 2020, **12**, 2023–2038.
14 A. Gupta, S. M. Briffa, S. Swingler, H. Gibson, V. Kannappan, G. Adamus, M. Kowalczuk, C. Martin and I. Radecka, *Biomacromolecules*, 2020, **21**, 1802–1811.
15 G. D. Winter, *Nature*, 1962, **193**, 293.
16 H. Geng, Q. Dai, H. Sun, L. Zhuang, A. Song, F. Caruso, J. Hao and J. Cui, *ACS Appl. Bio Mater.*, 2020, **3**, 1258–1266.
17 S. Tang, B. M. Richardson and K. S. Anseth, *Prog. Mater. Sci.*, 2021, **120**, 100738.
18 C. Ghobril and M. W. Grinstaff, *Chem. Soc. Rev.*, 2015, **44**, 1820–1835.
19 K. Chen, Q. Lin, L. Wang, Z. Zhuang, Y. Zhang, D. Huang and H. Wang, *ACS Appl. Mater. Interfaces*, 2021, **13**, 9748–9761.
20 C. W. Peak, J. J. Wilker and G. Schmidt, *Colloid Polym. Sci.*, 2013, **291**, 2031–2047.
21 B. Kaczmarek, A. Owczarek, K. Nadolna and A. Sionkowska, *Mater. Lett.*, 2019, **245**, 22–24.
22 J. Luo, J. Yang, X. Zheng, X. Ke, Y. Chen, H. Tan and J. Li, *Adv. Healthcare Mater.*, 2020, **9**, 1901423.
23 B. Liu, Y. Wang, Y. Miao, X. Zhang, Z. Fan, G. Singh, X. Zhang, K. Xu, B. Li, Z. Hu and M. Xing, *Biomaterials*, 2018, **171**, 83–96.
24 S. Yang, Y. Zhang, T. Wang, W. Sun and Z. Tong, *ACS Appl. Mater. Interfaces*, 2020, **12**, 46701–46709.
25 F. Sun, Y. Bu, Y. Chen, F. Yang, J. Yu and D. Wu, *ACS Appl. Mater. Interfaces*, 2020, **12**, 9132–9140.
26 Y. Li, R. Fu, C. Zhu and D. Fan, *Colloids Surf., B*, 2021, **205**, 111869.
27 M. Ma, Y. Zhong and X. Jiang, *Carbohydr. Polym.*, 2020, **236**, 116096.
28 M. Ma, Y. Zhong and X. Jiang, *J. Mater. Chem. B*, 2021, **9**, 4567–4576.
29 S. Guo, M. Yao, D. Zhang, Y. He, R. Chang, Y. Ren and F. Guan, *Adv. Healthcare Mater.*, 2022, 2101808.
30 Y. Yang, X. Zhao, J. Yu, X. Chen, R. Wang, M. Zhang, Q. Zhang, Y. Zhang, S. Wang and Y. Cheng, *Bioact. Mater.*, 2021, **6**, 3962–3975.
31 K. Kim, M. Shin, M.-Y. Koh, J. H. Ryu, M. S. Lee, S. Hong and H. Lee, *Adv. Funct. Mater.*, 2015, **25**, 2402–2410.
32 M. Shin, E. Park and H. Lee, *Adv. Funct. Mater.*, 2019, **29**, 1903022.
33 T. M. Shazly, A. B. Baker, J. R. Naber, A. Bon, K. J. Van Vliet and E. R. Edelman, *J. Biomed. Mater. Res., Part A*, 2010, **95**, 1159–1169.
34 J. Li, A. D. Celiz, J. Yang, Q. Yang, I. Wamala, W. Whyte, B. R. Seo, N. V. Vasilyev, J. J. Vlassak, Z. Suo and D. J. Mooney, *Science*, 2017, **357**, 378–381.
35 S. Bai, X. Zhang, P. Cai, X. Huang, Y. Huang, R. Liu, M. Zhang, J. Song, X. Chen and H.-H. Yang, *Nanoscale Horiz.*, 2019, **4**, 1333–1341.
36 G. Chen, Y. Yu, X. Wu, G. Wang, J. Ren and Y. Zhao, *Adv. Funct. Mater.*, 2018, **28**, 1801386.
37 Y. Wang, L. Li, Y. Ma, Y. Tang, Y. Zhao, Z. Li, W. Pu, B. Huang, X. Wen, X. Cao, J. Chen, W. Chen, Y. Zhou and J. Zhang, *ACS Nano*, 2020, **14**, 8202–8219.
38 D. Stern and H. Cui, *Adv. Healthcare Mater.*, 2019, **8**, 1900104.
39 H. Lei and D. Fan, *Chem. Eng. J.*, 2021, **421**, 129578.

40 Z. Wang, W. Hu, Y. Du, Y. Xiao, X. Wang, S. Zhang, J. Wang and C. Mao, *ACS Appl. Mater. Interfaces*, 2020, **12**, 13622–13633.
41 D. Mitra, M. Li, E.-T. Kang and K. G. Neoh, *ACS Appl. Mater. Interfaces*, 2019, **11**, 73–83.
42 P. Ren, H. Zhang, Z. Dai, F. Ren, Y. Wu, R. Hou, Y. Zhu and J. Fu, *J. Mater. Chem. B*, 2019, **7**, 5490–5501.
43 X. Zhao, P. Li, B. Guo and P. X. Ma, *Acta Biomater.*, 2015, **26**, 236–248.
44 T. Hao, J. Li, F. Yao, D. Dong, Y. Wang, B. Yang and C. Wang, *ACS Nano*, 2017, **11**, 5474–5488.
45 S. Zhang, J. Hou, Q. Yuan, P. Xin, H. Cheng, Z. Gu and J. Wu, *Chem. Eng. J.*, 2020, **392**, 123775.
46 M. Li, Z. Zhang, Y. Liang, J. He and B. Guo, *ACS Appl. Mater. Interfaces*, 2020, **12**, 35856–35872.
47 D. G. Barrett, G. G. Bushnell and P. B. Messersmith, *Adv. Healthcare Mater.*, 2013, **2**, 745–755.
48 N. Artzi, A. Zeiger, F. Boehning, A. bon Ramos, K. van Vliet and E. R. Edelman, *Acta Biomater.*, 2011, **7**, 67–74.
49 X. Zhao, D. Pei, Y. Yang, K. Xu, J. Yu, Y. Zhang, Q. Zhang, G. He, Y. Zhang, A. Li, Y. Cheng and X. Chen, *Adv. Funct. Mater.*, 2021, **31**, 2009442.
50 X. Zhao, Y. Liang, Y. Huang, J. He, Y. Han and B. Guo, *Adv. Funct. Mater.*, 2020, **30**, 1910748.
51 J. Chen, S. Li, Y. Zhang, W. Wang, X. Zhang, Y. Zhao, Y. Wang and H. Bi, *Adv. Healthcare Mater.*, 2017, **6**, 1700746.
52 S. Zhang, J. Hou, Q. Yuan, P. Xin, H. Cheng, Z. Gu and J. Wu, *Chem. Eng. J.*, 2020, **392**, 123775.
53 Y.-L. Huang and Y.-H. Tsai, *Int. J. Biol. Macromol.*, 2020, **160**, 677–687.
54 M. Anraku, J. M. Gebicki, D. Iohara, H. Tomida, K. Uekama, T. Maruyama, F. Hirayama and M. Otagiri, *Carbohydr. Polym.*, 2018, **199**, 141–149.

